Impact of Enteric Neuronal Loss on Intestinal Cell Composition

Naomi J.M. Kakiailatu[1], Laura E. Kuil[1], Jonathan D. Windster[1,2], Eric Bindels[3], Joke T.M. Zink[3], Michael Vermeulen[3], Bianca M. de Graaf[1], Deepavali Sahadew[1], Thierry P.P. van den Bosch[4], Demi Huijgen[2], Cornelius E.J. Sloots[2], Rene M.H. Wijnen[2], Robert M.W. Hofstra[1]†, Veerle Melotte[1,5] and Maria M. Alves[1,2]

[1]Department of Clinical Genetics, Erasmus University Medical Center, Sophia Children's Hospital, Rotterdam, The Netherlands.

[2]Department of Pediatric Surgery, Erasmus University Medical Center, Sophia Children's Hospital, Rotterdam, The Netherlands.

[3]Department of Hematology, Erasmus University Medical Center, Rotterdam, The Netherlands.

[4]Department of Pathology, Erasmus University Medical Center, Sophia Children's Hospital, Rotterdam, The Netherlands

[5]Department of Pathology, GROW- Research Institute for Oncology and Reproduction, Maastricht University Medical Center, Maastricht, The Netherlands.

Abstract

Hirschsprung disease (HSCR) is a congenital disorder characterized by the absence of an enteric nervous system (ENS) in the distal gut, causing obstruction and constipation. Despite the known importance of the ENS for normal gut function due to its interaction with other intestinal cells, the impact of ENS loss on intestinal homeostasis remains largely unexplored. In this manuscript, we investigate changes in intestinal composition associated with loss of an ENS, by performing single cell RNA sequencing on zebrafish intestines collected from 5 days post-fertilization wildtype zebrafish and a *ret* mutant HSCR model. Significant findings were validated through immunofluorescence and fluorescence *in situ* hybridization in zebrafish and human tissues. Notable shifts included a reduction in enterocytes and enterochromaffin cells, alongside an increase in immune and endothelial cells, as well as BEST4+ enterocytes, in the HSCR model. These discoveries elucidate significant changes in the intestinal cellular composition in HSCR, highlighting potential pathways to secondary complications and offering insights into new therapeutic possibilities aimed at enhancing patient outcomes.

Keywords: Single-cell RNA sequencing, Zebrafish intestine, Non-neuronal cells, Hirschsprung disease (HSCR), Enteric nervous system (ENS)

Introduction

The enteric nervous system (ENS) is a large network that consists of neurons and glia. The ENS not only controls intestinal motility but is also responsible for a diverse range of functions within the intestine. This includes facilitating communication with various intestinal cell types, thereby influencing mucosal transport and secretions. Additionally, the ENS plays a significant role in modulating immune and endocrine responses as well as regulating blood flow within the intestinal system (1). The ENS arises from enteric neural crest cells (ENCC) which migrate along the gut, proliferate and differentiate to colonize the whole intestine (1, 2). Defects in any of these processes can lead to gastrointestinal dysmotility disorders associated with a variety of enteric neuropathies (3). Hirschsprung disease (HSCR) is the most common congenital enteric neuropathy, occurring approximately in one in 5.000 newborns (4, 5). HSCR is characterized by the lack of enteric neurons in the colon, most commonly in the distal part, resulting in intestinal constipation and obstruction (1, 6). The length of the affected segment varies and is referred to as the aganglionic segment. In 70-80% of the cases only the rectum and sigmoid colon are affected, resulting in short segment HSCR. Long segment HSCR occurs when the aganglionic part extends beyond the sigmoid or descending colon junction, and total colonic aganglionosis (TCA) occurs when the entire colon is affected (5, 7).

HSCR is a complex multi-genetic disease, but the most important gene involved in its pathogenesis is the Rearranged during transfection gene (*RET*). *RET* codes for a transmembrane tyrosine kinase receptor that is expressed in ENCCs, supporting their survival, proliferation, differentiation, and migration (8, 9). Pathogenic variants in *RET* account for 50% of familial and 15% of sporadic cases (10, 11). Until now, more than 30 HSCR genes have been identified, but together they explain merely 30% of all the cases, suggesting the presence of missing heritability in HSCR.

The standard treatment for HSCR is pull-through surgery, in which the aganglionic part of the colon is removed. This surgery is performed in the first few months of life (12-14). Although this procedure is life-saving, it is not curative and is accompanied by secondary complications in 32% of the patients (15). Early complications include anastomotic leak, enterocolitis, perianal excoriation and adhesional obstruction. Long-term complications are associated with chronic obstructive symptoms, enterocolitis and soiling. Furthermore, up to 10% of children diagnosed with HSCR may require a colostomy or further surgery to treat constipation or incontinence. These clinical symptoms strongly indicate a persistent problem in the ganglionic region of the colon and rectum, which remains even after the surgical removal of the affected bowel segment (16, 17). This can not only suggest a possible impairment of the ENS in the ganglionic bowel, but also the potential involvement of other

intestinal cell types. However, up to date limited studies have focus on the interaction between the ENS and other intestinal cells during development and disease pathogenesis.

In this study, we aim to investigate which intestinal cell types are affected due to absence of the ENS. For this, we performed single cell RNA sequencing (scRNA-seq) on isolated intestines from both wildtype and *ret* mutant zebrafish, with a total colonic HSCR phenotype. The cellular changes observed might account for the secondary complications diagnosed in HSCR patients and may even play a role in the efficiency of new future treatment options.

Results

Characterization of different intestinal cell types present in zebrafish

The goal of this study is to explore the impact of enteric neuronal loss on other intestinal cell types. To do so, we first characterized the transcriptomic profile from 5 days post fertilization (dpf) wildtype zebrafish intestines (Figure 1A) In total, 244 intestines were isolated and 9200 cells were captured. We identified 48 clusters in total, which were grouped into 12 cell types based on their expression markers (Supplementary figure 1A, Figure 1B, 1C). Although we tried to selectively isolate the intestine, some contamination of liver and pancreas tissue was observed in cluster 30, 38 and 47. One of the most abundant cell types identified, including clusters 0, 1, 3, 4, 12 and 30, seemed to be mesenchymal cells present in the extracellular matrix (ECM), mainly expressing collagen-containing ECM genes (*col1a2, col1a1, dcn, aspn*). Cluster 0 is represented by fibroblasts, expressing the fibroblast marker *vim* and ECM components (*col1a2, col1a1, cxcl12a*). Cluster 1 and 3 are characterized by *wnt* and *rspo* expression, known to be secreted by stromal myofibroblasts, which are responsible for stem cell homeostasis regulation (18). Cluster 4 is characterized by *cxcl12a* expression, which is a stromal secreted factor and exhibits chemoattractant activity (19). Cluster 12 seems to consist of stromal cells, expressing several collagen genes, but also *spon2b*, predicted to be involved in cell adhesion and located in the ECM (20).

Another significant population present was the epithelial population, primarily composed of enterocytes (*fabp2, mogat2*), identified in cluster 6 and 22 (21, 22). Cluster 32 and 37 consisted of enteroendocrine cells (*neurod1, cldnh, ccka*) and a small cluster of enterochromaffin cells (EECs) (*tph1a, tph1b*) was identified in cluster 48. (23, 24). Furthermore, BEST4+ enterocytes (*best4, otop2, anxa4*, *cftr*) were present in cluster 17, and a small population of goblet cells was identified in cluster 41 (*agr2, sstr5*) (25-27). *Sstr5* stimulates mucin2 expression in the colon, but was also described as critical for protection of the intestinal barrier function during colitis (28). Interestingly, *sstr5* was found to also be expressed in the BEST4+ enterocyte population. Additionally, we uncovered epithelial progenitors in cluster 28, 35 and 41. These clusters expressed *epcam*, a known marker for epithelial cells, involved in cell signaling, migration, proliferation and differentiation (29-31).

Clusters 5, 13, 29 and 45 consist predominantly of leukocytes expressing markers such as *lcp1, coro1a, ccl38.1* (32-34). Notably, in zebrafish innate immune cell types emerge as early as 15 hours post-fertilization (hpf), while adaptive immune cells emerge only after 7 dpf (35-38). Noteworthy, the expression of *ccr9a* in cluster 2 suggests the potential presence of developing T cells. This chemokine receptor is known to be involved in the trafficking of T cells to the gut-associated lymphoid tissue, indicating its significance in immune responses,

particularly in the intestinal environment (39). Furthermore, macrophages (*mpeg, mfap4*) were identified in cluster 11, which are known to emerge from 1 dpf (40, 41).

Clusters 9, 19, 20 and 39 consist of neuronal and glial cells. Neuronal progenitor cells (*phox2bb, sox10, elavl3/4, slc1a2b*) and Schwann cell progenitors (*mmp17b, clic6, sox10*) were identified, as well as more differentiated neurons expressing *vip/nos*, sensory neurons *(nmu, vgf, tac3a and calb2a)* and glia (*her4.2.1, her4.1, cx43*) (42). These neuronal and glial clusters were extensively described before (42). Additionally, clusters 14, 18, 25 and 33 consisted of muscle cells (*acta2, tagln, mylkb, tpm2)*, cluster 36 of thrombocytes (*itga2b, f5, mpl*) and cluster 7, 15, 21 and 40 of endothelial cells (*kdrl, flt1, flk4, stab1*) (43-50)

Differential cellular composition in ret mutant zebrafish intestine

To explore the impact of enteric neuronal loss on other intestinal cell types, we performed scRNA-seq on 5 dpf *ret*$^{hu2846/hu2846}$ tg(*phox2bb*:GFP) zebrafish intestines, which we referred to as *ret* mutants. These *ret* mutant zebrafish showed a total colonic HSCR phenotype (Figure 2A). In total, 266 intestines were isolated and 10.326 cells were captured. To integrate both wildtype and *ret* mutant datasets, we down-sampled them to 9200 cells each for equitable comparisons. This approach ensured a balanced and unbiased comparison between the two conditions. Subsequently, a permutation test was performed to evaluate changes in cell proportions between wildtype and *ret* mutant zebrafish intestines (Figure 2B, C). As expected, a decrease of ENS cells was observed in the *ret* mutant zebrafish. However, our analysis showed that other intestinal cell types were also affected. The most prominent differences were observed in immune cells, endothelial cells and epithelial cells. Additionally, clusters related to the ECM were marginally affected, except cluster 12, composed by a distinct population of stromal cells within the ECM (*spon2b*, *hoxa13b*, *efemp2b*, *fgfbp2a*, and *hoxd12a* genes), was completely absent in the *ret* mutant zebrafish. No differences were observed in the abundance of smooth muscle cells in the *ret* mutant zebrafish.

Increased immune cell populations in ret mutant zebrafish intestine

Eleven distinct subclusters were identified in the subset analysis of the immune cell populations (Figure 3A). These subclusters predominantly consisted of leukocytes, immune progenitors, differentiating immune cells, and macrophages, reflecting the underdeveloped state of the adaptive immune system in 5 dpf zebrafish. Notably, the scRNA-seq analysis depicted an increase of immune cell numbers within the *ret* mutant zebrafish (1462 vs. 2312 cells). This increase affected almost all immune subclusters, especially the immune progenitor cells expressing *csf1rb, cxcr4b,* and *myb*. Importantly, no significant changes

were identified in the number of macrophages defined by *mpeg* and *mfap4* expression (Figure 3B).

To validate the elevated immune cell population in the *ret* mutant zebrafish *in vivo*, we performed whole-mount immunohistochemistry (IHC) stainings on both wildtype and *ret* mutant zebrafish using L-plastin, a leukocyte marker expressed in all immune clusters (Figure 3C). An increased number of Lcp+ cells was detected in *ret* mutants (p = 0.005) (Figure 3D, E), confirming the scRNA-seq results.

Endothelial cell dynamics in ret mutant zebrafish intestine

In addition to the immune cell alterations, a significant increase in the endothelial cell populations was observed in the *ret* mutant zebrafish intestines compared to the wildtypes (334 vs 1331) (Supplementary figure 1B). To validate this result, the tg(*kdrl*:mcherry) transgenic line was used, as *kdrl* is a crucial gene for vascular development and is expressed in all endothelial cells. Live-imaging of wildtype tg(*kdrl*:mcherry) and *ret* tg(*kdrl*:mcherry) zebrafish was performed, and we were able to visualize and compare the vascular structures of both wildtype and *ret* mutant zebrafish (Supplementary figure 1C). However, no significant differences were detected in structure or number of *kdrl* positive cells between the wildtype and *ret* mutant zebrafish *in vivo* (Supplementary figure 1D).

Changes in epithelial cell types in ret mutant zebrafish Intestine

Sub-analysis of epithelial cell types showed prominent alterations in the epithelial cell composition of the *ret* mutant zebrafish compared to the wildtypes (Figure 4A). Fourteen distinct clusters were identified, including epithelial progenitor cells (*epcam, her15*), BEST4+ enterocytes and two minor populations of goblet cells (*agr2*), and ECCs (*tph1a, tph1b*). Enterocytes were further classified into 6 clusters, with Enterocytes 1, 2, and 4 expressing genes characteristic of the anterior region of the gut (*fabp2, ada, fabp1b.1, vil1*), and Enterocytes 3 expressing mid-region genes (*fabp6, slc10a2, tmigd1*) (27). Enterocytes 5 exhibited a more progenitor-like profile (*epcam, sult6b1, wnt11r*) and Enterocytes 6 was identified with proliferating markers (*mki67, cdk1, top2a, fabp2*) (27). Additionally, 3 enteroendocrine clusters were identified. The Enteroendocrine 1 cluster expressed hormones that regulates glucose metabolism (*gcga, gcgb*) (51). Enteroendocrine 2 was characterized by *ccka*, which regulates gut motility, satiety, and lipid and protein digestion and Enteroendocrine 3 expressed more progenitor-like markers, such as *neurod1* and *pax6b* (52-55).

Specifically, the enterocytes population showed a significant reduction, with only 304 cells present in the *ret* mutants, compared to 785 in the wildtypes (Figure 4B). Similarly, a significant reduction of ECCs was observed in the *ret* mutants (ECCs; 29 vs 1 cell). *In situ*

hybridization using a *fabp2* probe to identify enterocytes and a 5HT IHC staining to quantify ECCs, confirmed the reduction of both cell types in the *ret* mutant zebrafish (p=3.518E-05) (Figure 4C,D,E).

An increase of BEST4+ enterocytes was also detected in the scRNA-seq data in the *ret* mutant zebrafish, when compared to wildtype (49 vs 258 cells) (Figure 5A). This difference was validated with fluorescent in situ hybridization (FISH) for *best4*, and interestingly, an increase of these cells was specifically detected in the distal part of the intestine, as BEST4+ enterocytes were totally absent in this region in wildtype zebrafish but not in *ret* mutants (Figure 5B,C).

Translational Relevance: Human validations

In order to assess the translational relevance of our findings in zebrafish, we conducted IHC analyses in human tissue targeting specific cell types affected in our zebrafish HSCR model. Tissue samples were obtained from a cohort comprising four healthy controls and five HSCR patients, all of whom exhibited a *RET* mutation and were clinically diagnosed with total colonic aganglionosis (Table 1).

By performing immunostainings for 5HT, we were able to reveal a statistically significant decrease in ECCs in HSCR patients, when compared to the healthy controls (p = 0.0027), (Figure 6A, B). Additionally, immunofluorescence analysis targeting CD45, a pan-leukocyte marker indicative of cells in both the innate and adaptive immune systems, demonstrated a substantial increase in CD45+ immune cells within the HSCR patient cohort (p = 0.008), (Figure 6C, D). These results align with our zebrafish model outcomes.

We also assess the presence of BEST4+ enterocytes through quantification via IHC, and our results revealed a decrease in the number of BEST4+ cells in HSCR patients compared to healthy controls (Figure 7A, B). This result was opposite to the one observed with the *ret* mutant as an increase of Best4 cells was observed.

Discussion

Here we present the single-cell transcriptomic profile of 5 dpf zebrafish intestines, where we identified a diverse range of intestinal cell types including immune, endothelial, muscle, epithelial, and ENS cells. Importantly, by comparing control intestines with those of *ret* mutant zebrafish presenting with a phenotype reminiscent of total colonic HSCR in humans, distinct alterations in intestinal composition were observed, which were validated *in vivo*. Our findings extend beyond the zebrafish, as we demonstrate their translational relevance to humans, providing additional validation of an altered human intestinal composition in the absence of an ENS.

One of the most serious complications in HSCR patients is Hirschsprung-associated enterocolitis (HAEC), but its underlying mechanisms remain poorly understood (56, 57). HAEC is characterized by inflammatory colitis with symptoms ranging from distension, diarrhea, and fever to potentially fatal outcomes (58). It occurs both pre- and post- surgery, implying that the pathogenic mechanisms of HAEC extend beyond the aganglionic region and are likely to involve an altered intestinal barrier function and mucosal immune responses (59). Also, numerous studies have shown that the ENS plays a pivotal role in modulating immune responses within the intestinal microenvironment (60). This intricate communication between the ENS and the immune system extends its relevance to non-infectious gastrointestinal disorders, particularly inflammatory bowel disease (IBD) (60-63). Our study showed a significant increase in immune progenitor cells in the intestines of *ret* mutant zebrafish even at an early developmental stage and in the absence of external stimuli, such as feeding. An increase in immune cells was also observed in intestinal tissue from HSCR patients, suggesting that the absence of ENS contributes to an imbalanced immune response, that may well influence the onset of enterocolitis. Moreover, we observed an altered epithelial composition in the *ret* mutant zebrafish intestines. Since *ret* has been described to sustain proliferation and tissue maturation of the intestinal epithelium, this result aligns with its expected functions (64). A significant decrease of ECCs was observed, which was validated in zebrafish and HSCR patients. ECCs are located alongside the epithelium and are amongst other things, responsible for synthesizing and secreting serotonin. They contribute significantly to gastrointestinal regulation, particularly to intestinal motility and secretion (65, 66). *ret* is expressed in a subset of ECCs, which might explain the decreased number of these cells in the *ret* mutant zebrafish (64). In the context of HSCR, these findings imply that alterations in *RET* expression could impact ECCs and serotonin production, potentially influencing gastrointestinal dysmotility associated with the disease. However, it's noteworthy that inhibiting Ret kinase activity in adult mice did not affect serotonin levels, indicating that the specific effects of *ret* on ECCs may vary across developmental stages

and/or species (67). This insight into the relationship between *ret*, ECCs, and intestinal function provides a basis for further exploration of potential therapeutic targets or interventions, aimed at modulating ECCs and serotonin signaling in HSCR patients.

Enterocytes, crucial for nutrient absorption, showed a decrease in the *ret* mutant zebrafish, which we validated using ISH. However, our attempts to validate the presence of enterocytes in human tissue were hindered by limited access to small intestinal tissue samples. *Fabp2*, a marker for enterocytes, is predominantly expressed in the small intestine, and aganglionic segments are usually colon. Without location matched samples, direct comparison of enterocyte abundance between healthy controls and HSCR patients, is currently not feasible. The recently described BEST4+ enterocytes were also identified in our dataset. BEST4+ enterocytes are absorptive epithelial cells, which play a role in luminal pH regulation, suggesting a supportive role for optimal microbial growth (25). BEST4+ enterocytes are also a source of uroguanylin, regulating intestinal electrolyte balance, through guanylyl cyclase C (GC-C) receptor activation. Dysfunction of this pathway is known to impact epithelial barrier function and cause intestinal inflammation. In our data, an increased number of BEST4+ enterocytes was detected in the *ret* mutant zebrafish model. Remarkably, *best4*+ cells were absent from the most posterior part of the wildtype zebrafish gut, whereas in *ret* mutant zebrafish, these cells were present throughout the entire gut. In HSCR patients however, we observed a reduced number of BEST4+ enterocytes in the aganglionic region. This is in line with previous scRNA-seq data showing loss of BEST4+ enterocytes in other intestinal diseases, such as IBD and colon carcinoma (25, 68, 69). Considering that the presence and location of BEST4+ enterocytes in humans appears to be highly influenced by factors such as age and intestinal location, it is difficult to make direct comparisons. Moreover, since the number of *best4*+ cells primarily differed in the distal part of the zebrafish gut, and there is limited access to rectum tissue from healthy control patients, direct comparison of our results in human samples is challenging. Also, at 5 dpf the zebrafish are at a developmental stage that doesn't directly align with the pediatric age of the human tissue used. It is important to address these limitations to fully understand the impact of our zebrafish findings, and to improve our knowledge on the composition of the intestine in HSCR patients. Nevertheless, we believe that understanding the role of enterocytes in HSCR, remains vital for potential therapeutic interventions.

Our scRNA-seq data also indicated an increased number of endothelial cells in the *ret* mutant zebrafish intestines. However, due to the complex nature of blood vessel formation, we were unable to validate this finding *in vivo* using the transgenic *kdrl* zebrafish line. Nonetheless, our scRNA-seq results are consistent with a previous report showing a significant increase in microvascular density in the aganglionic region of HSCR patients (70). A strong interaction between the vascular system and the ENS has also been previously

suggested, with enteric neurons migrating alongside blood vessels during the establishment of the neuronal network of the gut (71). However, studies in mice with impaired microvasculature have demonstrated that enteric neurons can colonize the gut even in the absence of blood vessels, while mice without an ENS showed a normal vascular network suggesting that both networks develop independently (72).

Overall, our analysis did not reveal significant differences in ECM clusters. However, a specific group of stromal cells in the ECM, known as cluster 12, was completely absent in the intestines of the *ret* mutant zebrafish. This cluster is characterized by the expression of several collagen genes, but also *spon2b* and *c1qtnf5*, which are predicted to be involved in cell adhesion (20, 73)**.** Previous research underscores the role of the ECM in maintaining tissue homeostasis and contributing to ENS development (74-78). For instance, β1 integrins, found on the cell surface of ENCCs, have been shown to facilitate ENCC migration by interacting with ECM proteins expressed by the intestinal vasculature (79). Additionally, recent scRNA-seq studies highlight ECM alterations and a fibrotic phenotype in aganglionic segments of HSCR patients (80), further suggesting potential shifts in ECM composition specific to this condition. Further studies should be performed to explore the identity of this cluster and its potential involvement in HSCR pathogenesis

In conclusion, our in-depth single-cell transcriptomic analysis of 5 dpf wildtype and *ret* mutant zebrafish intestines has unraveled crucial insights into the cellular composition and alterations associated with HSCR disease. The validations of our findings in intestinal tissue samples from aganglionic regions of HSCR patients carrying a *RET* mutation, underscores the clinical relevance of our results, providing a comprehensive understanding of the intestinal complications linked to HSCR. These findings, also open up new avenues for potential therapeutic interventions. Considering the observed changes in cellular composition, therapies that target immune modulation, and strategies to optimize epithelial cell composition, such as anti-inflammatory medications and probiotics, could be explored. Importantly, our study holds promise for improving transplantation therapies, by optimizing the intestinal environment through targeted interventions. This not only enhances the understanding and treatment of primary complications in HSCR, but could also have implications for preventing secondary complications, such as enterocolitis.

Materials and methods

Animal husbandry

The following zebrafish lines were used: transgenic tg(*phox2bb*:GFP) (81), tg(*kdrl*:mcherry) (82), and *ret*$^{hu2846/+}$ (83). Zebrafish were kept on a 14/10h light/dark cycle. Embryos and larvae were kept in an incubator at 28.5^{o}C in HEPES-buffered E3 medium. For imaging experiments, fish were treated from 24 hpf onwards with 0.2 mM 1-phenyl 2-thiourea (PTU), to inhibit pigmentation. Animal experiments were approved by the Animal Experimentation Committee of the Erasmus MC, Rotterdam (AVD1010020209425).

Isolation of zebrafish intestines and pre-processing of intestinal cell suspension for single cell RNA sequencing

Intestines of 5 dpf wildtype and *ret* mutant tg(phox2bb:GFP) zebrafish were isolated and dissociated as described before (84, 85). In total, 244 intestines of the wildtypes and 266 intestines of the *ret* mutant zebrafish, were isolated and dissociated using papain as a dissociation enzyme.

Single cell RNA sequencing analysis of the zebrafish cells using Seurat

scRNA-seq analysis was performed using Seurat V3 as described before (86-89). Datasets obtained for the intestines of 5 dpf wildtype and *ret* mutant zebrafish were integrated for analysis. The *ret* mutant dataset consisted of 10.326 cells and was down-sampled to 9200 cells to obtain an equal number of cells. The Seurat pipeline was used for filtering (nFeature_RNA > 100 & nFeature_RNA <4200 & percent.mito < 0.05) normalization, integration and downstream analysis. We used 50 dimensions with a resolution of 0.8 for the clustering, and UMAP for the processing of the individual datasets, as well as for the post-processing of the merged dataset.

Immune and epithelial sub-analysis using Seurat

For the immune subset analysis, clusters 2, 5, 11, 13, 29, and 45 were selected. We used 20 dimensions with a clustering resolution of 0.5 for both clustering and UMAP visualization, resulting in 14 clusters. Clusters 6 and 10, which likely represented ECM and epithelial contamination, were intentionally excluded. The final analysis was conducted using 10 dimensions and a resolution of 0.5, yielding eleven clusters.

For the epithelial subset analysis, we specifically selected clusters 6, 17, 22, 28, 32, 35, 37, 41, 42, 43, 44, and 48. We again used 20 dimensions with a clustering resolution of 0.5 resulting in 18 clusters. Exclusion criteria involved clusters 9 and 15, indicative of ECM

and immune contamination. The final analysis was performed with 8 dimensions and a resolution of 0.5.

Sub-cluster annotation was performed based on differential gene expression and literature review.

Zebrafish Immunohistochemistry

Whole mount IHC using rabbit anti-LCP1 (1:200, Genetex GTX124420) was performed, as previously described (83). Antibody staining using rabbit anti-5HT (1:200, Immunostar 20080) was performed as described before (90). Zebrafish were fixed in 4% PFA, dehydrated in 70% ethanol, and processed with a blocking solution (0.2% BSA, 0.5% Triton X-100, 1% DMSO, 5% horse serum, PBS). They were incubated overnight with primary antibody at 4°C, followed by overnight anti-rabbit Cy3 (1:250, Jackson) incubation. Finally, they were stained with DAPI for 3 minutes and stored in PBS at 4°C.

Zebrafish Whole-mount *in situ* hybridization

Whole mount *in situ* hybridization (WISH) with Digoxyigenin (DIG)-labeled was performed using standard protocols, as described previously (91). In short, 5 dpf wildtype and *ret* mutant zebrafish were fixed in 4% PFA, dehydrated in a graded methanol series (0%/25%/50%/100%), and subsequent rehydrated. To permeabilize the zebrafish, they underwent a 15 minute protein K treatment at 28,5°C, followed by refixation, and prehybridization at 65°C. Hybridization with denatured probes occurred overnight at 65°C, followed by post-hybridization washes. Blocking preceded an overnight incubation with Roche anti-DIG antibody. Subsequent washes, staining in 5µL NBT/BCIP per mL, and a stop solution were performed. After clearing in 50% glycerol/PBST, embryos were stored in glycerol.

Fabp2 probe was designed with the following sequence: Antisense probe: aattaatacgactcactataGGCTTTAGGGCTGCCAATCATTAAAGC. Sense probe: TACGAGAAGTTCATGGAACAAATGG. Images were taken using the Olympus SZX1 microscope.

Zebrafish Whole-mount fluorescent *in situ* hybridization

Whole-mount fluorescent *in situ* hybridization (FISH) was performed as described before (42) The RNAscope Multiplex Fluorescence Reagent Kit v2 Assay (Advanced Cell Diagnostics, Bio-Techne) was used according to the manufacturers' instructions. A custom-made probe for dr-*best4* C1 was used (NPR-0035110, Advanced Cell Diagnostics, Bio-Techne). Opal 570 dye (Akoya Biosciences) was used for channel development.

Live imaging zebrafish

Confocal imaging was performed using the SP5 intravital microscope with a 20x water-dipping lens, as previously described (92). Imaging of the 5 dpf tg(*phox2bb*:GFP; *kdrl*:mcherry) zebrafish was performed using the 488 nm and 561 nm laser. Briefly, zebrafish were anesthetized with 0.016% MS-222 in HEPES-buffered E3 and securely positioned in a row within low-melting agarose for stability during imaging. The imaging dish containing the embedded zebrafish was filled with HEPES-buffered E3 containing 0.016% MS-222.

Quantification of IHC and FISH stainings in zebrafish

The number of immune cells, endothelial cells, ECCs and BEST4+ enterocytes were manually counted through the Z-stack projections using FIJI (93). Length of the gut was measured using the straight-line tool. The number of counted cells was normalized to the gut length.

Human IHC and confocal microcopy

Supplemental Table 1 describes the diagnosis and major characteristics of all donors included in this study. Immunofluorescence for CD45 (1:200 #AMAb90518, Atlas Antibodies) and 5HT (1:200 #20080, Immunostar) was performed on pediatric tissue blocks obtained from the Department of Pathology of the Erasmus Medical Center, as previous described (89). Shortly, 4 µm sections were cut, deparaffinized using xylene and a graded ethanol series, followed by a pressure cooker treatment in 0.01M sodium citrate. Primary antibody was incubated overnight at 4°C and secondary antibody was incubated for 1 hour at room temperature. Anti-rabbit Cy3 (1:200, Jackson) was used for the 5HT stainings and anti-mouse Alexa 488 (1:200, Jackson) for the CD45 stainings. Finally, DAPI staining was applied for 1 minute. The slides were then rinsed and mounted using a fluorescence mounting medium. Confocal imaging for 5HT, CD45 and FABP2 was performed using the Stellaris confocal microscope with both 20x and 40x lense.

The BEST4 stainings were performed by automated IHC using the Ventana Benchmark ULTRA (Ventana Medical Systems Inc.). Sequential 4 µm thick (FFPE) sections were stained using optiview (OV) (#760-700, Ventana). In brief, following deparaffinization and heat-induced antigen retrieval with CC1 (#950-500, Ventana) for 32 minutes the tissue samples were incubated with BEST4 (1:100 #HPA058564, Atlas Antibodies) for 32 minutes at 37˚C. Incubation was followed by optiview detection and hematoxylin II counter stain for 8 minutes followed by a blue coloring reagent for 8 minutes according to the manufactures instructions (Ventana). The BEST4 slides were scanned using the Nanozoomer slide scanner (Hamamatsu) at the Pathology department of the Erasmus Medical Center.

Image analysis and quantification of human IHC stainings

Image analysis and quantification of human IHC stainings involved manual counting of 5HT cells per crypt using FIJI (93). For CD45, a FIJI threshold was applied, and counts were determined per square, with 5 equal squares analyzed per slide. QuPath was used for BEST4 staining quantifications (94). Epithelial regions were selected to facilitate automated cell counting. Only the cone-shaped cells present in the epithelium were considered as BEST4+ cells.

Statistical analysis

For proportion testing of the scRNA-seq datasets of wildtype and *ret* mutant zebrafish, Seurat was used. Significant changes were determined with a permutation test to calculate p-values for each cluster. A confidence interval for the magnitude difference was returned via bootstrapping. p value <0.05 was considered significant. Paired t-tests were performed to compare the mean cell counts between wildtype and *ret* mutant zebrafish, as well as for each staining comparing human controls and HSCR patients.

Declaration of generative AI and AI-assisted technologies in the writing process

During the preparation of this work the author(s) used ChatGPT in order to improve language and grammar of the manuscript. After using this tool/service, the author(s) reviewed and edited the content as needed and take(s) full responsibility for the content of the publication

References

1. Wallace AS, Burns AJ. Development of the enteric nervous system, smooth muscle and interstitial cells of Cajal in the human gastrointestinal tract. Cell Tissue Res. 2005;319(3):367-82.
2. Nagy N, Goldstein AM. Enteric nervous system development: A crest cell's journey from neural tube to colon. Semin Cell Dev Biol. 2017;66:94-106.
3. Goldstein AM, Thapar N, Karunaratne TB, De Giorgio R. Clinical aspects of neurointestinal disease: Pathophysiology, diagnosis, and treatment. Dev Biol. 2016;417(2):217-28.
4. Parisi MA, Kapur RP. Genetics of Hirschsprung disease. Curr Opin Pediatr. 2000;12(6):610-7.
5. Badner JA, Sieber WK, Garver KL, Chakravarti A. A genetic study of Hirschsprung disease. Am J Hum Genet. 1990;46(3):568-80.
6. Whitehouse FR, Kernohan JW. Myenteric plexus in congenital megacolon; study of 11 cases. Arch Intern Med (Chic). 1948;82(1):75-111.
7. Kawaguchi AL, Guner YS, Somme S, Quesenberry AC, Arthur LG, Sola JE, et al. Management and outcomes for long-segment Hirschsprung disease: A systematic review from the APSA Outcomes and Evidence Based Practice Committee. J Pediatr Surg. 2021;56(9):1513-23.
8. Natarajan D, Marcos-Gutierrez C, Pachnis V, de Graaff E. Requirement of signalling by receptor tyrosine kinase RET for the directed migration of enteric nervous system progenitor cells during mammalian embryogenesis. Development. 2002;129(22):5151-60.
9. Taraviras S, Marcos-Gutierrez CV, Durbec P, Jani H, Grigoriou M, Sukumaran M, et al. Signalling by the RET receptor tyrosine kinase and its role in the development of the mammalian enteric nervous system. Development. 1999;126(12):2785-97.
10. Attie T, Pelet A, Edery P, Eng C, Mulligan LM, Amiel J, et al. Diversity of RET proto-oncogene mutations in familial and sporadic Hirschsprung disease. Hum Mol Genet. 1995;4(8):1381-6.
11. Angrist M, Bolk S, Halushka M, Lapchak PA, Chakravarti A. Germline mutations in glial cell line-derived neurotrophic factor (GDNF) and RET in a Hirschsprung disease patient. Nat Genet. 1996;14(3):341-4.
12. Swenson O, Neuhauser EB, Pickett LK. New concepts of the etiology, diagnosis and treatment of congenital megacolon (Hirschsprung's disease). Pediatrics. 1949;4(2):201-9.
13. Soave F. Hirschsprung's Disease: A New Surgical Technique. Arch Dis Child. 1964;39(204):116-24.
14. Duhamel B. [New operation for congenital megacolon: retrorectal and transanal lowering of the colon, and its possible application to the treatment of various other malformations]
Une nouvelle operation pour le megacolon congenital: l'abaissement retro-rectal et trans-anal du colon et son application possible au traitement de quelques autres malformations. Presse Med (1893). 1956;64(95):2249-50.
15. M E, S A. Obstructive complications after pull-through for Hirschsprung's disease: different causes and tailored management. Annals of Pediatric Surgery. 2019.
16. Hackam DJ, Filler RM, Pearl RH. Enterocolitis after the surgical treatment of Hirschsprung's disease: risk factors and financial impact. J Pediatr Surg. 1998;33(6):830-3.
17. Moore SW, Albertyn R, Cywes S. Clinical outcome and long-term quality of life after surgical correction of Hirschsprung's disease. J Pediatr Surg. 1996;31(11):1496-502.
18. Sigal M, Logan CY, Kapalczynska M, Mollenkopf HJ, Berger H, Wiedenmann B, et al. Stromal R-spondin orchestrates gastric epithelial stem cells and gland homeostasis. Nature. 2017;548(7668):451-5.
19. Mueller A, Meiser A, McDonagh EM, Fox JM, Petit SJ, Xanthou G, et al. CXCL4-induced migration of activated T lymphocytes is mediated by the chemokine receptor CXCR3. J Leukoc Biol. 2008;83(4):875-82.

20. Lu H, Feng Y, Hu Y, Guo Y, Liu Y, Mao Q, et al. Spondin 2 promotes the proliferation, migration and invasion of gastric cancer cells. J Cell Mol Med. 2020;24(1):98-113.
21. Weiss EP, Brown MD, Shuldiner AR, Hagberg JM. Fatty acid binding protein-2 gene variants and insulin resistance: gene and gene-environment interaction effects. Physiol Genomics. 2002;10(3):145-57.
22. Zhou YG, Yin RX, Huang F, Wu JZ, Chen WX, Cao XL. DGAT2-MOGAT2 SNPs and Gene-Environment Interactions on Serum Lipid Profiles and the Risk of Ischemic Stroke. Front Cardiovasc Med. 2021;8:685970.
23. Krentz NAJ, Lee MYY, Xu EE, Sproul SLJ, Maslova A, Sasaki S, et al. Single-Cell Transcriptome Profiling of Mouse and hESC-Derived Pancreatic Progenitors. Stem Cell Reports. 2018;11(6):1551-64.
24. Ye L, Bae M, Cassilly CD, Jabba SV, Thorpe DW, Martin AM, et al. Enteroendocrine cells sense bacterial tryptophan catabolites to activate enteric and vagal neuronal pathways. Cell Host Microbe. 2021;29(2):179-96 e9.
25. Parikh K, Antanaviciute A, Fawkner-Corbett D, Jagielowicz M, Aulicino A, Lagerholm C, et al. Colonic epithelial cell diversity in health and inflammatory bowel disease. Nature. 2019;567(7746):49-55.
26. Haber AL, Biton M, Rogel N, Herbst RH, Shekhar K, Smillie C, et al. A single-cell survey of the small intestinal epithelium. Nature. 2017;551(7680):333-9.
27. Willms RJ, Jones LO, Hocking JC, Foley E. A cell atlas of microbe-responsive processes in the zebrafish intestine. Cell Reports. 2022;38(5):110311.
28. Li Y, Li X, Geng C, Guo Y, Wang C. Somatostatin receptor 5 is critical for protecting intestinal barrier function in vivo and in vitro. Mol Cell Endocrinol. 2021;535:111390.
29. Gonzalez B, Denzel S, Mack B, Conrad M, Gires O. EpCAM is involved in maintenance of the murine embryonic stem cell phenotype. Stem Cells. 2009;27(8):1782-91.
30. Ng VY, Ang SN, Chan JX, Choo AB. Characterization of epithelial cell adhesion molecule as a surface marker on undifferentiated human embryonic stem cells. Stem Cells. 2010;28(1):29-35.
31. Maghzal N, Vogt E, Reintsch W, Fraser JS, Fagotto F. The tumor-associated EpCAM regulates morphogenetic movements through intracellular signaling. J Cell Biol. 2010;191(3):645-59.
32. Dubey M, Singh AK, Awasthi D, Nagarkoti S, Kumar S, Ali W, et al. L-Plastin S-glutathionylation promotes reduced binding to beta-actin and affects neutrophil functions. Free Radic Biol Med. 2015;86:1-15.
33. Kaminski S, Hermann-Kleiter N, Meisel M, Thuille N, Cronin S, Hara H, et al. Coronin 1A is an essential regulator of the TGFbeta receptor/SMAD3 signaling pathway in Th17 CD4(+) T cells. J Autoimmun. 2011;37(3):198-208.
34. Zhou Q, Zhao C, Yang Z, Qu R, Li Y, Fan Y, et al. Cross-organ single-cell transcriptome profiling reveals macrophage and dendritic cell heterogeneity in zebrafish. Cell Rep. 2023;42(7):112793.
35. Bennett CM, Kanki JP, Rhodes J, Liu TX, Paw BH, Kieran MW, et al. Myelopoiesis in the zebrafish, Danio rerio. Blood. 2001;98(3):643-51.
36. Carradice D, Lieschke GJ. Zebrafish in hematology: sushi or science? Blood. 2008;111(7):3331-42.
37. de Jong JL, Zon LI. Use of the zebrafish system to study primitive and definitive hematopoiesis. Annu Rev Genet. 2005;39:481-501.
38. Traver D, Herbomel P, Patton EE, Murphey RD, Yoder JA, Litman GW, et al. The zebrafish as a model organism to study development of the immune system. Adv Immunol. 2003;81:253-330.
39. Uehara T, Park JT. Role of the murein precursor UDP-N-acetylmuramyl-L-Ala-gamma-D-Glu-meso-diaminopimelic acid-D-Ala-D-Ala in repression of beta-lactamase induction in cell division mutants. J Bacteriol. 2002;184(15):4233-9.
40. Ellett F, Pase L, Hayman JW, Andrianopoulos A, Lieschke GJ. mpeg1 promoter transgenes direct macrophage-lineage expression in zebrafish. Blood. 2011;117(4):e49-56.

41. Walton EM, Cronan MR, Beerman RW, Tobin DM. The Macrophage-Specific Promoter mfap4 Allows Live, Long-Term Analysis of Macrophage Behavior during Mycobacterial Infection in Zebrafish. PLoS One. 2015;10(10):e0138949.
42. Kuil LE, Kakiailatu NJM, Windster JD, Bindels E, Zink JTM, van der Zee G, et al. Unbiased characterization of the larval zebrafish enteric nervous system at a single cell transcriptomic level. iScience. 2023;26(7):107070.
43. Perrin BJ, Ervasti JM. The actin gene family: function follows isoform. Cytoskeleton (Hoboken). 2010;67(10):630-4.
44. Li L, Miano JM, Cserjesi P, Olson EN. SM22 alpha, a marker of adult smooth muscle, is expressed in multiple myogenic lineages during embryogenesis. Circ Res. 1996;78(2):188-95.
45. Hardeman EC, Bryce NS, Gunning PW. Impact of the actin cytoskeleton on cell development and function mediated via tropomyosin isoforms. Semin Cell Dev Biol. 2020;102:122-31.
46. Faucherre A, Kissa K, Nargeot J, Mangoni ME, Jopling C. Piezo1 plays a role in erythrocyte volume homeostasis. Haematologica. 2014;99(1):70-5.
47. Stull JT, Kamm KE, Vandenboom R. Myosin light chain kinase and the role of myosin light chain phosphorylation in skeletal muscle. Arch Biochem Biophys. 2011;510(2):120-8.
48. Emambokus N, Vegiopoulos A, Harman B, Jenkinson E, Anderson G, Frampton J. Progression through key stages of haemopoiesis is dependent on distinct threshold levels of c-Myb. EMBO J. 2003;22(17):4478-88.
49. Gurung S, Restrepo NK, Chestnut B, Klimkaite L, Sumanas S. Single-cell transcriptomic analysis of vascular endothelial cells in zebrafish embryos. Sci Rep. 2022;12(1):13065.
50. Zygmunt T, Gay CM, Blondelle J, Singh MK, Flaherty KM, Means PC, et al. Semaphorin-PlexinD1 signaling limits angiogenic potential via the VEGF decoy receptor sFlt1. Dev Cell. 2011;21(2):301-14.
51. Gribble FM, Reimann F. Enteroendocrine Cells: Chemosensors in the Intestinal Epithelium. Annu Rev Physiol. 2016;78:277-99.
52. Le H, Lie KK, Giroud-Argoud J, Ronnestad I, Saele O. Effects of Cholecystokinin (CCK) on Gut Motility in the Stomachless Fish Ballan Wrasse (Labrus bergylta). Front Neurosci. 2019;13:553.
53. Rehfeld JF. Cholecystokinin-From Local Gut Hormone to Ubiquitous Messenger. Front Endocrinol (Lausanne). 2017;8:47.
54. Li HJ, Ray SK, Pan N, Haigh J, Fritzsch B, Leiter AB. Intestinal Neurod1 expression impairs paneth cell differentiation and promotes enteroendocrine lineage specification. Sci Rep. 2019;9(1):19489.
55. Hill ME, Asa SL, Drucker DJ. Essential requirement for Pax6 in control of enteroendocrine proglucagon gene transcription. Mol Endocrinol. 1999;13(9):1474-86.
56. Demehri FR, Halaweish IF, Coran AG, Teitelbaum DH. Hirschsprung-associated enterocolitis: pathogenesis, treatment and prevention. Pediatr Surg Int. 2013;29(9):873-81.
57. Aslam A, Spicer RD, Corfield AP. Children with Hirschsprung's disease have an abnormal colonic mucus defensive barrier independent of the bowel innervation status. J Pediatr Surg. 1997;32(8):1206-10.
58. Lewit RA, Kuruvilla KP, Fu M, Gosain A. Current understanding of Hirschsprung-associated enterocolitis: Pathogenesis, diagnosis and treatment. Semin Pediatr Surg. 2022;31(2):151162.
59. Li S, Zhang Y, Li K, Liu Y, Chi S, Wang Y, et al. Update on the Pathogenesis of the Hirschsprung-Associated Enterocolitis. International Journal of Molecular Sciences. 2023;24(5):4602.
60. Wang H, Foong JPP, Harris NL, Bornstein JC. Enteric neuroimmune interactions coordinate intestinal responses in health and disease. Mucosal Immunol. 2022;15(1):27-39.
61. Yoo BB, Mazmanian SK. The Enteric Network: Interactions between the Immune and Nervous Systems of the Gut. Immunity. 2017;46(6):910-26.

62. Sanovic S, Lamb DP, Blennerhassett MG. Damage to the Enteric Nervous System in Experimental Colitis. The American Journal of Pathology. 1999;155(4):1051-7.
63. Margolis KG, Stevanovic K, Karamooz N, Li ZS, Ahuja A, D'Autreaux F, et al. Enteric neuronal density contributes to the severity of intestinal inflammation. Gastroenterology. 2011;141(2):588-98, 98 e1-2.
64. Perea D, Guiu J, Hudry B, Konstantinidou C, Milona A, Hadjieconomou D, et al. Ret receptor tyrosine kinase sustains proliferation and tissue maturation in intestinal epithelia. EMBO J. 2017;36(20):3029-45.
65. Rehfeld JF. A centenary of gastrointestinal endocrinology. Horm Metab Res. 2004;36(11-12):735-41.
66. Sternini C, Anselmi L, Rozengurt E. Enteroendocrine cells: a site of 'taste' in gastrointestinal chemosensing. Curr Opin Endocrinol Diabetes Obes. 2008;15(1):73-8.
67. Shepherd A, Feinstein L, Sabel S, Rastelli D, Mezhibovsky E, Matthews L, et al. RET Signaling Persists in the Adult Intestine and Stimulates Motility by Limiting PYY Release from Enteroendocrine Cells. bioRxiv. 2022.
68. Smillie CS, Biton M, Ordovas-Montanes J, Sullivan KM, Burgin G, Graham DB, et al. Intra- and Inter-cellular Rewiring of the Human Colon during Ulcerative Colitis. Cell. 2019;178(3):714-30 e22.
69. Zhang L, Yu X, Zheng L, Zhang Y, Li Y, Fang Q, et al. Lineage tracking reveals dynamic relationships of T cells in colorectal cancer. Nature. 2018;564(7735):268-72.
70. Schrenk S, Schuster A, Klotz M, Schleser F, Lake J, Heuckeroth RO, et al. Vascular and neural stem cells in the gut: do they need each other? Histochemistry and Cell Biology. 2015;143(4):397-410.
71. Nagy N, Mwizerwa O, Yaniv K, Carmel L, Pieretti-Vanmarcke R, Weinstein BM, et al. Endothelial cells promote migration and proliferation of enteric neural crest cells via beta1 integrin signaling. Dev Biol. 2009;330(2):263-72.
72. Delalande JM, Natarajan D, Vernay B, Finlay M, Ruhrberg C, Thapar N, et al. Vascularisation is not necessary for gut colonisation by enteric neural crest cells. Dev Biol. 2014;385(2):220-9.
73. Tu X, Palczewski K. The macular degeneration-linked C1QTNF5 (S163) mutation causes higher-order structural rearrangements. Journal of Structural Biology. 2014;186(1):86-94.
74. Nakazawa-Tanaka N, Fujiwara N, Miyahara K, Nakada S, Arikawa-Hirasawa E, Akazawa C, et al. The effect of laminin-1 on enteric neural crest-derived cell migration in the Hirschsprung's disease mouse model. Pediatr Surg Int. 2018;34(2):143-7.
75. Nagy N, Barad C, Graham HK, Hotta R, Cheng LS, Fejszak N, et al. Sonic hedgehog controls enteric nervous system development by patterning the extracellular matrix. Development. 2016;143(2):264-75.
76. Soret R, Mennetrey M, Bergeron KF, Dariel A, Neunlist M, Grunder F, et al. A collagen VI-dependent pathogenic mechanism for Hirschsprung's disease. J Clin Invest. 2015;125(12):4483-96.
77. Nishida S, Yoshizaki H, Yasui Y, Kuwahara T, Kiyokawa E, Kohno M. Collagen VI suppresses fibronectin-induced enteric neural crest cell migration by downregulation of focal adhesion proteins. Biochem Biophys Res Commun. 2018;495(1):1461-7.
78. Nagy N, Barad C, Hotta R, Bhave S, Arciero E, Dora D, et al. Collagen 18 and agrin are secreted by neural crest cells to remodel their microenvironment and regulate their migration during enteric nervous system development. Development. 2018;145(9).
79. Nagy N, Barad C, Graham H, Hotta R, Cheng L, Fejszak N, et al. Sonic hedgehog controls enteric nervous system development by patterning the extracellular matrix. Development. 2015;143(2):264-75.
80. He S, Wang J, Huang Y, Kong F, Yang R, Zhan Y, et al. Intestinal fibrosis in aganglionic segment of Hirschsprung's disease revealed by single-cell RNA sequencing. Clinical and Translational Medicine. 2023;13(2).
81. Nechiporuk A, Linbo T, Poss KD, Raible DW. Specification of epibranchial placodes in zebrafish. Development. 2007;134(3):611-23.

82. Bertrand JY, Chi NC, Santoso B, Teng S, Stainier DY, Traver D. Haematopoietic stem cells derive directly from aortic endothelium during development. Nature. 2010;464(7285):108-11.
83. Heanue TA, Boesmans W, Bell DM, Kawakami K, Vanden Berghe P, Pachnis V. A Novel Zebrafish ret Heterozygous Model of Hirschsprung Disease Identifies a Functional Role for mapk10 as a Modifier of Enteric Nervous System Phenotype Severity. PLoS Genet. 2016;12(11):e1006439.
84. Kuil LE, Kakiailatu NJM, Windster JD, Bindels E, Zink JTM, van der Zee G, et al. Unbiased characterization of the larval zebrafish enteric nervous system at a single cell transcriptomic level. iScience. 2023;26(7).
85. Kakiailatu NJM, Kuil LE, Bindels E, Zink JTM, Vermeulen M, Melotte V, et al. Gut Isolation from Zebrafish Larvae for Single-cell RNA Sequencing. J Vis Exp. 2023(201).
86. Satija R, Farrell JA, Gennert D, Schier AF, Regev A. Spatial reconstruction of single-cell gene expression data. Nat Biotechnol. 2015;33(5):495-502.
87. Butler A, Hoffman P, Smibert P, Papalexi E, Satija R. Integrating single-cell transcriptomic data across different conditions, technologies, and species. Nat Biotechnol. 2018;36(5):411-20.
88. Stuart T, Butler A, Hoffman P, Hafemeister C, Papalexi E, Mauck WM, 3rd, et al. Comprehensive Integration of Single-Cell Data. Cell. 2019;177(7):1888-902 e21.
89. Windster JD, Kuil LE, Kakiailatu NJM, Antanaviciute A, A. S, C. M, et al. Human enteric glia diversity in health and disease: new avenues for the treatment of Hirschsprung disease. BioRxiv. 2023.
90. Hyland C, Mfarej M, Hiotis G, Lancaster S, Novak N, Iovine MK, et al. Impaired Cx43 gap junction endocytosis causes morphological and functional defects in zebrafish. Mol Biol Cell. 2021;32(20):ar13.
91. Thisse C, Thisse B. High-resolution in situ hybridization to whole-mount zebrafish embryos. Nat Protoc. 2008;3(1):59-69.
92. Kuil LE, Oosterhof N, Ferrero G, Mikulášová T, Hason M, Dekker J, et al. Zebrafish macrophage developmental arrest underlies depletion of microglia and reveals Csf1r-independent metaphocytes. eLife. 2020;9:e53403.
93. Schneider CA, Rasband WS, Eliceiri KW. NIH Image to ImageJ: 25 years of image analysis. Nat Methods. 2012;9(7):671-5.
94. Bankhead P, Loughrey MB, Fernandez JA, Dombrowski Y, McArt DG, Dunne PD, et al. QuPath: Open source software for digital pathology image analysis. Sci Rep. 2017;7(1):16878.

Figure legends

Figure 1. Transcriptomic profile of the wildtype zebrafish intestine at 5 dpf.

A) Experimental design of isolated zebrafish intestines for scRNA-seq. Intestines of 5 dpf wildtype tg(*phox2bb*:GFP) zebrafish were isolated and enzymatically dissociated. FACS was used to sort live, single cells for scRNA-seq. B) UMAP of intestinal cells, containing 12 different cell types. Every dot represents a cell which are color coded by cell type. C) Dot plot showing expression of genes highly differentially expressed between clusters.

Figure 2. Altered intestinal composition in *ret* mutant zebrafish larvae.

A) Schematic representation of the *ret* mutant tg(*phox2bb*:GFP) zebrafish gut isolation for scRNA-seq. B) UMAP of wildtype and *ret* mutant zebrafish showing differences in intestinal composition. C) Differences between cell proportions in clusters identified for wildtype and *ret* mutant intestines. Error-bars represent the variability within each cluster.

Figure 3. Immune cells are increased in ret mutant zebrafish.

A) UMAP of immune cell sub-analysis, containing 11 clusters. B) Featureplot showing *lcp1* expression in wildtype and *ret* mutant datasets. C) Proportion table showing cell proportions per cluster between wildtype and *ret* mutant datasets. C) IHC staining of LCP1 in tg(*phoxbb*:GFP) wildtype and *ret* mutant zebrafish, showing increased numbers of LCP1+ cells in the *ret* mutant zebrafish. Representative maximum projections from 5 dpf larvae. The intestine is marked by the white dashed lines. Phox2bb+ cells are shown in green and LCP1+ cells in red, depicted by the white arrowheads. Scale bar represents 80 µm. D) Graph showing significant increased numbers of LCP1+ cells in *ret* mutant zebrafish.

Figure 4. Altered epithelial composition in *ret* mutant zebrafish larvae.

A) UMAP of epithelial sub-analysis in wildtype and *ret* mutant zebrafish, containing 12 clusters. B) Featureplot showing *fabp*2 expression in wildtype and *ret* mutant datasets. C) *In situ* hybridization of *fabp2* in wildtype and *ret* mutant zebrafish. D) Maximum projections of immunohistochemistry staining of 5HT in tg(*phox2bb*:GFP) wildtype and *ret* mutant zebrafish. Intestines are marked by the white dashed lines. Phoxbb+ cells are shown in green and 5HT+ cells in magenta. Scale bar represents 80 µm. E) Graph showing decreased numbers of 5HT+ cells in *ret* mutant zebrafish.

Figure 5. Increased number of *best4*+ enterocytes in *ret* mutant zebrafish larvae.

A) Featureplot of *best4* expression in wildtype and *ret* mutant zebrafish datasets. Fluorescent *in situ* hybridization of *best4* in tg(*phox2bb*:GFP) wildtype and *ret* mutant zebrafish. B) Representative maximum projections from 5 dpf wildtype and *ret* mutant tg(*phox2bb*:GFP) zebrafish. Intestines are marked by the white dashed lines. Phox2bb+ cells are highlighted in green and *best4*+ cells in magenta. Arrows indicate the presence of *best4*+ enterocytes presence. C) Quantification of the number of *best4*+ cells in both anterior and posterior regions of the intestine, in wildtype and *ret* mutant zebrafish.

Figure 6. Immunohistochemical validation and quantification in tissue collected from HSCR patients.

A) IHC validation of 5HT in control and HSCR aganglionic tissue. DAPI is shown in grey and 5HT+ cells in magenta. Scale bar represents 100 µm. B) Graph showing significant decrease of 5HT+ cells/ per crypt in aganglionic tissue of HSCR patients. C) IHC validation of CD45+ cells in control and HSCR aganglionic tissue. DAPI is depicted in grey and CD45+ cells in red. Scale bar represents 100 µm. D) Graph showing significant increase of CD45+ cells in HSCR aganglionic tissue.

Figure 7. Decrease of BEST4+ enterocytes in HSCR patients.

A) IHC staining for BEST4 in control and HSCR aganglionic tissue. Arrows depict BEST4+ enterocytes. B) Graph showing significant decrease of BEST4+ enterocytes in aganglionic tissue of HSCR patients.

Acknowledgments

We thank Iain Shepherd (Department of Biology, Emory University, Atlanta, USA) and Kaushal Parikh (Department of Gastroenterology and Hepatology, Erasmus University Medical Center, Rotterdam, NL) for their valuable feedback on the manuscript. We also thank Remko Hoogenboezem (Department of Hematology) for processing our raw single-cell data, Emma de Pater (Department of Hematology, Erasmus MC) for the scRNA-seq script, and the optical imaging center (OIC) of the Erasmus University Medical Center (Rotterdam, NL) for assistance with confocal microscopy. This work was funded by the Friends of the Sophia Foundation (SSWO WAR-63).

Consent for Publication

Not applicable

Author contributions statement

NJMK, LEK, RMWH, VM and MMA designed and planned the experiments; NJMK, LEK, JDW, JTMZ, MV, BMdG and DS prepared and executed the experiments; NJMK, LEK and EB supervised, prepared and analysed the single cell RNA sequencing data; TPPvdB provided human intestinal biopsies; DH, CEJS and RMWH provided clinical information; VM, and MMA provided supervision and guidance; NJMK, LEK, VM and MMA interpreted the data and wrote the manuscript.

Conflict of Interest Statement

The authors declare no competing interest

Data and materials availability

The raw and processed data used for this study will be available in NCBIs Gene Expression Omnibus through the GEO series accession number. Any additional information required to reanalyze the data reported in this paper is available upon request.

Figure 1

A

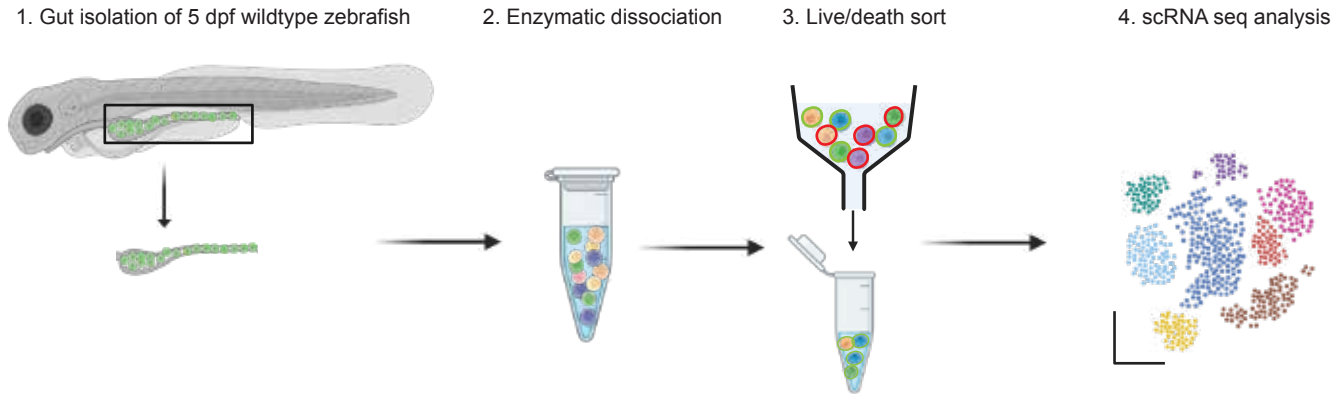
1. Gut isolation of 5 dpf wildtype zebrafish
2. Enzymatic dissociation
3. Live/death sort
4. scRNA seq analysis

B

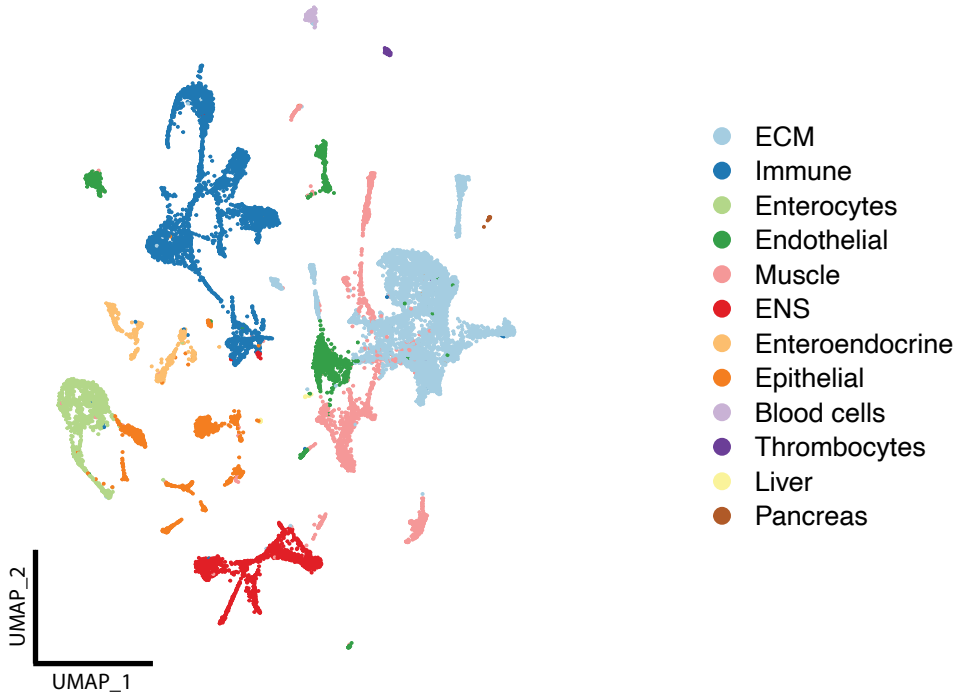
ECM
Immune
Enterocytes
Endothelial
Muscle
ENS
Enteroendocrine
Epithelial
Blood cells
Thrombocytes
Liver
Pancreas
UMAP_2
UMAP_1

C

Pancreas
Liver
Thrombocytes
Blood cells
Epithelial
Enteroendocrine
ENS
Muscle
Endothelial
Enterocytes
Immune
ECM
col1a2
dcn
aspn
lcp1
coro1a
ccl38.1
fabp2
stab1
flt4
kdrl
acta2
myod1
mylkb
phox2bb
sox10
elavl3
gck
pax6b
neurod1
best4
epcam
hbbe1.2
cobll1a
fabp10a
dkk1b
Average Expression
2.5
2.0
1.5
1.0
0.5
0.0
−0.5
Percent Expressed
0
25
50
75

Figure 2

A

Gut isolation of 5 dpf *ret* mutant zebrafish

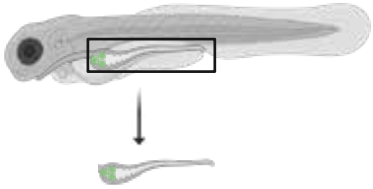

B

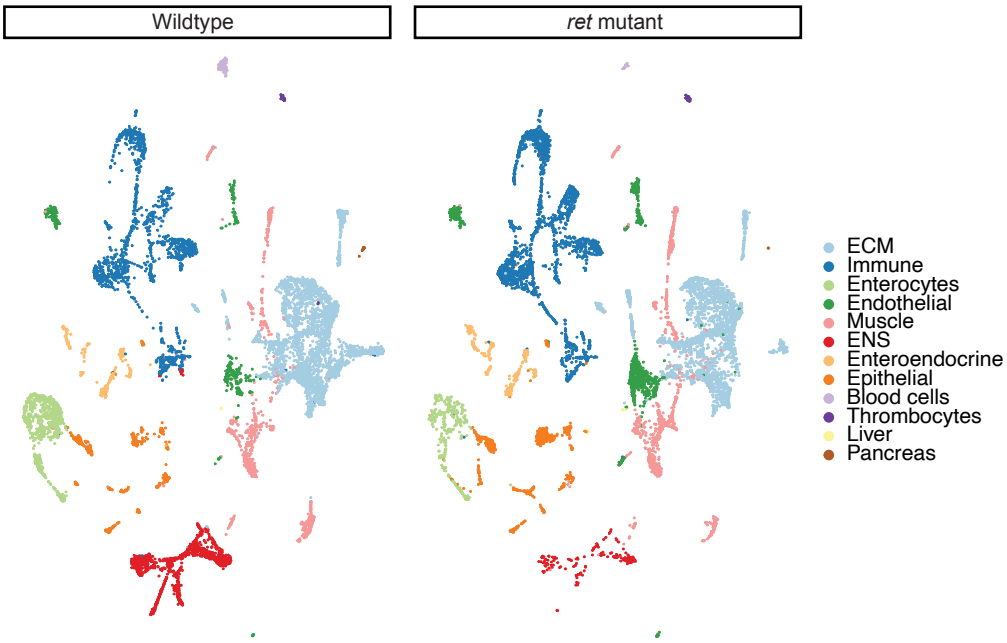

C

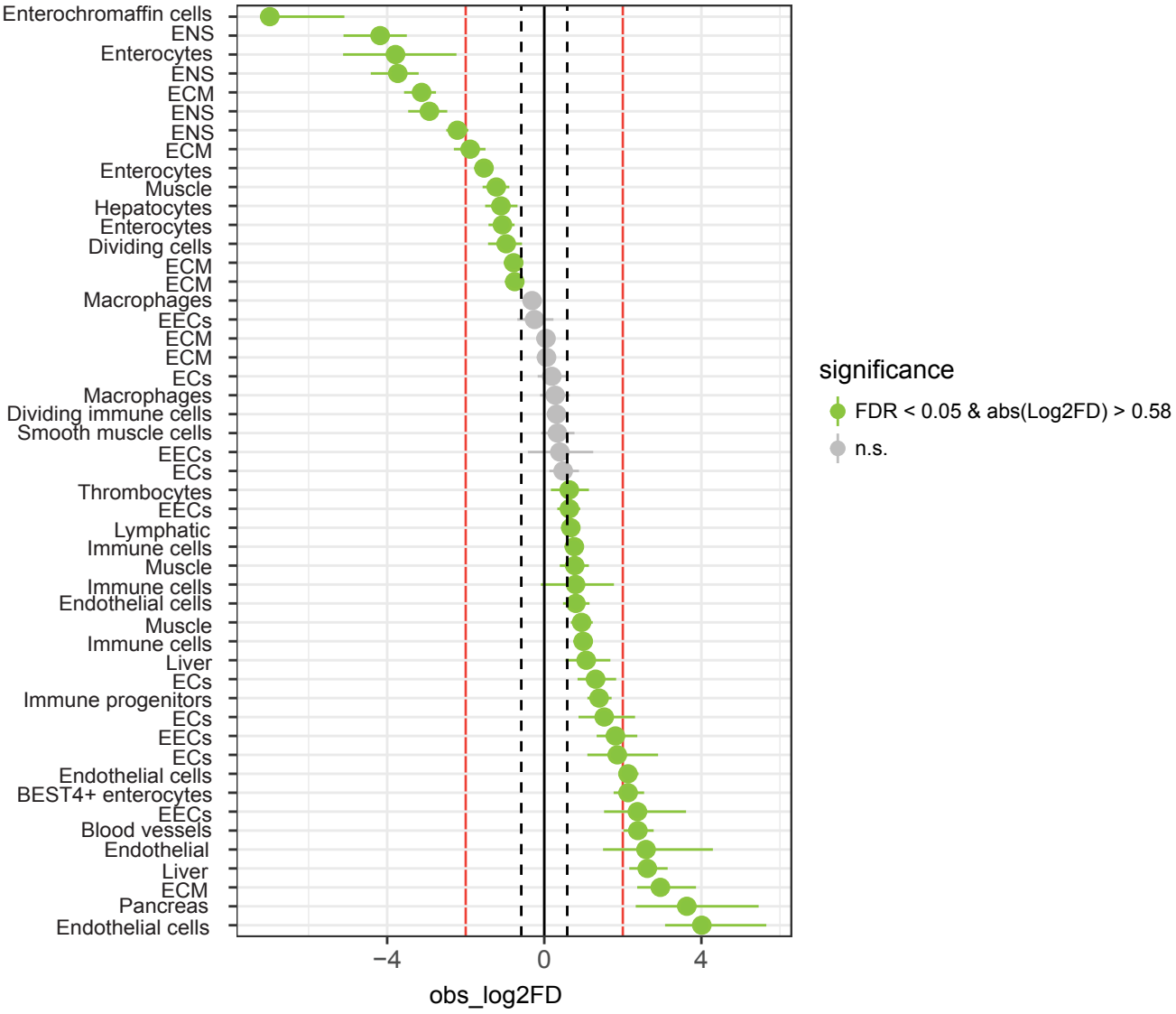

Figure 3

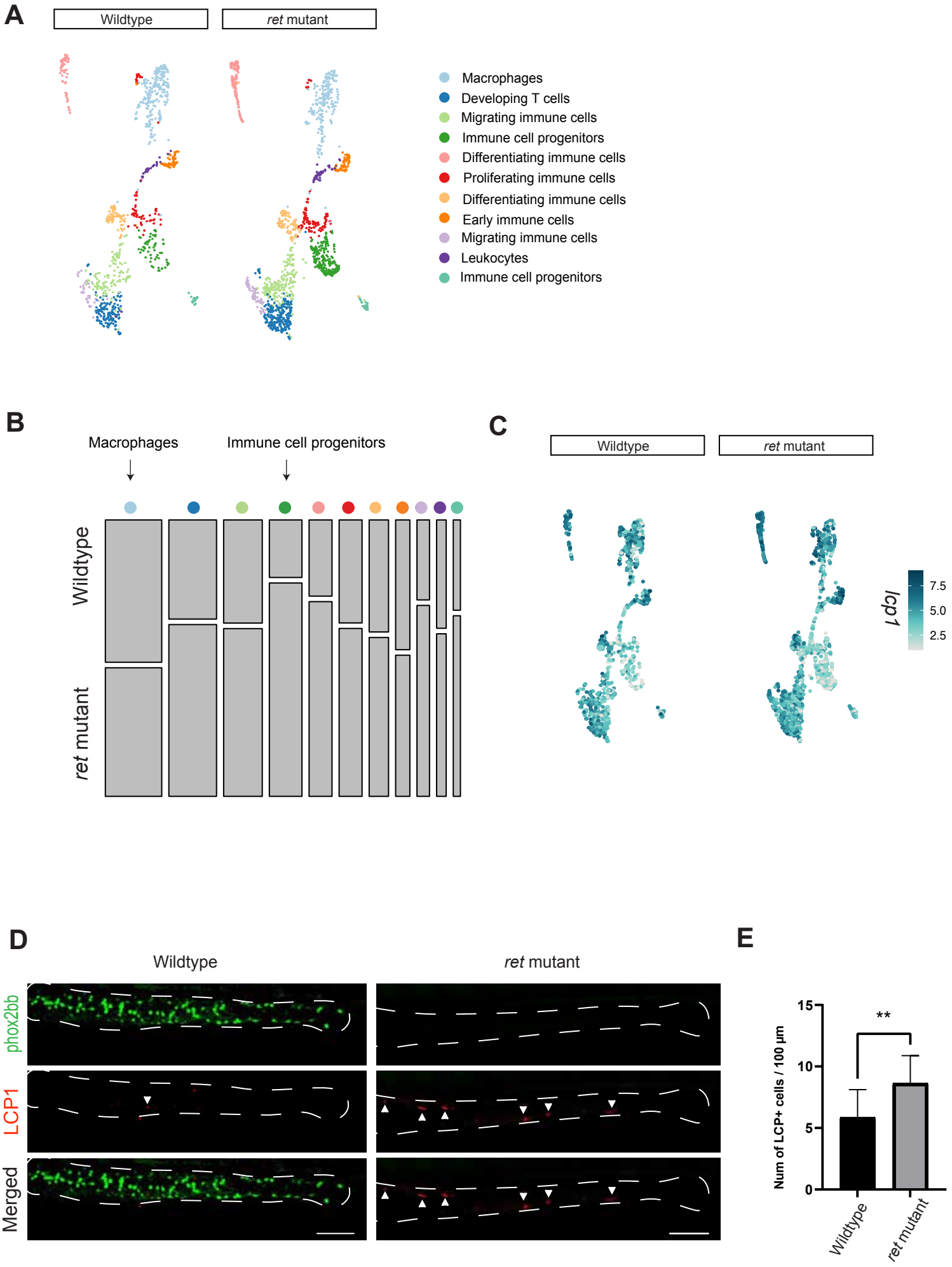
A
Wildtype
ret mutant
Macrophages
Developing T cells
Migrating immune cells
Immune cell progenitors
Differentiating immune cells
Proliferating immune cells
Differentiating immune cells
Early immune cells
Migrating immune cells
Leukocytes
Immune cell progenitors
B
Macrophages
Immune cell progenitors
Wildtype
ret mutant
C
Wildtype
ret mutant
lcp1
7.5
5.0
2.5
D
Wildtype
ret mutant
phox2bb
LCP1
Merged
E
Num of LCP+ cells / 100 µm
15
10
5
0
**
Wildtype
ret mutant

Figure 4

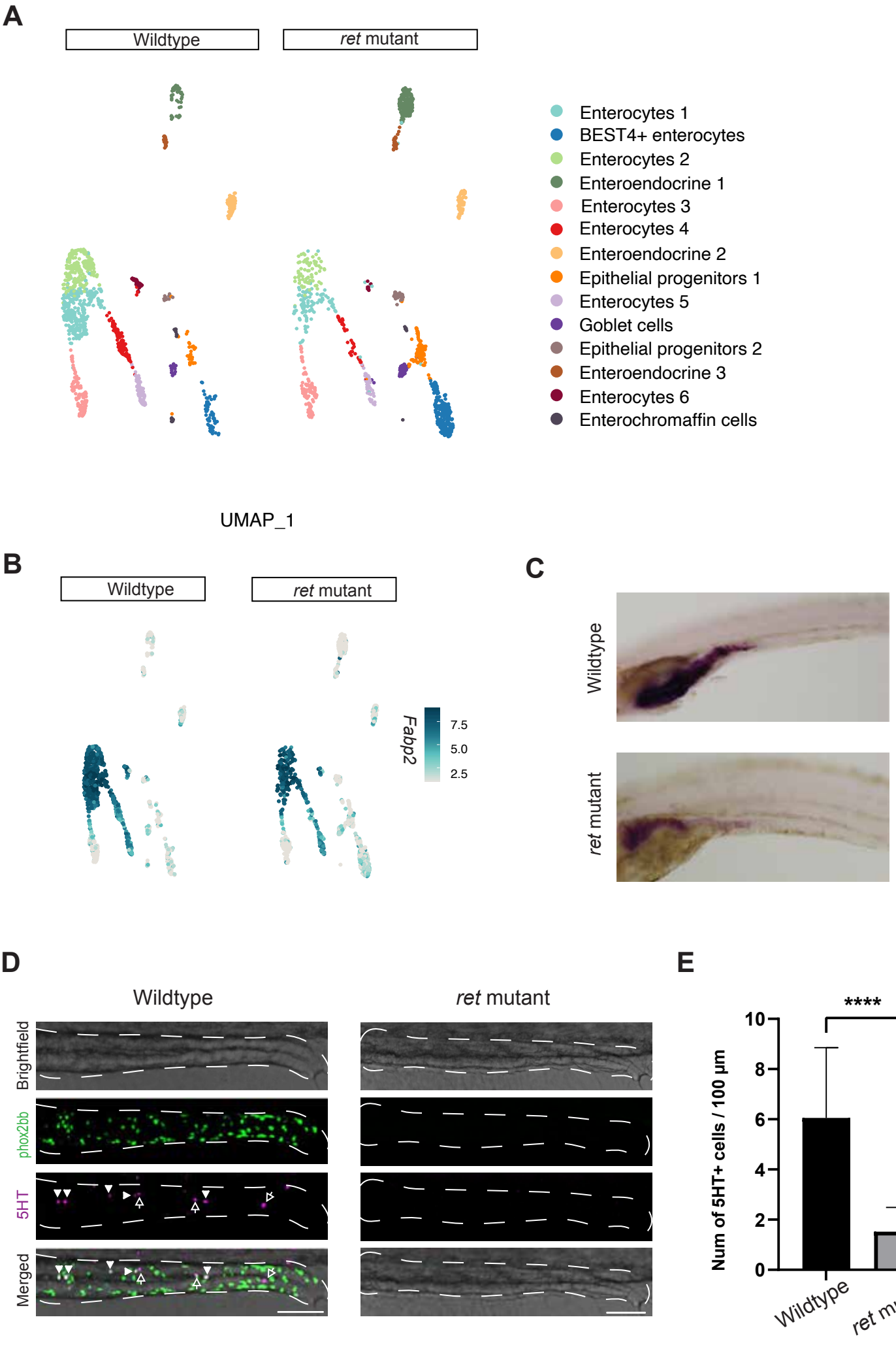
A
Wildtype
ret mutant
Enterocytes 1
BEST4+ enterocytes
Enterocytes 2
Enteroendocrine 1
Enterocytes 3
Enterocytes 4
Enteroendocrine 2
Epithelial progenitors 1
Enterocytes 5
Goblet cells
Epithelial progenitors 2
Enteroendocrine 3
Enterocytes 6
Enterochromaffin cells
UMAP_1
B
Wildtype
ret mutant
Fabp2
7.5
5.0
2.5
C
Wildtype
ret mutant
D
Wildtype
ret mutant
Brightfield
phox2bb
5HT
Merged
E
****
Num of 5HT+ cells / 100 µm
10
8
6
4
2
0
Wildtype
ret mutant

Figure 5

A

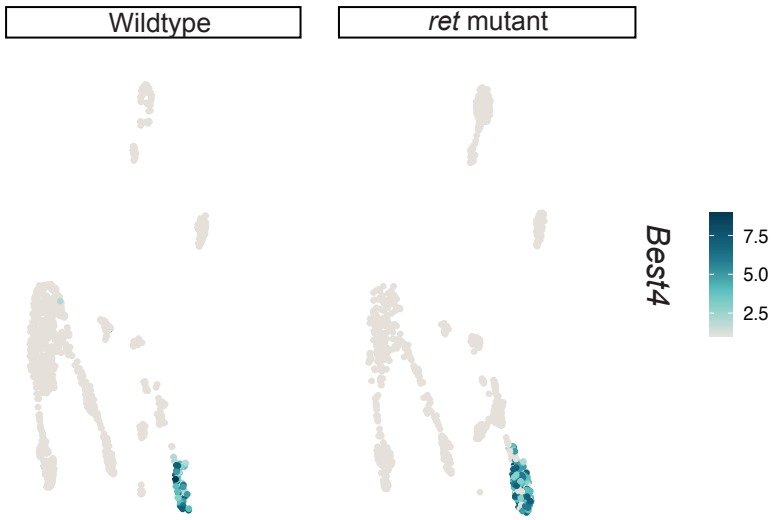
Wildtype
ret mutant
Best4
7.5
5.0
2.5

B

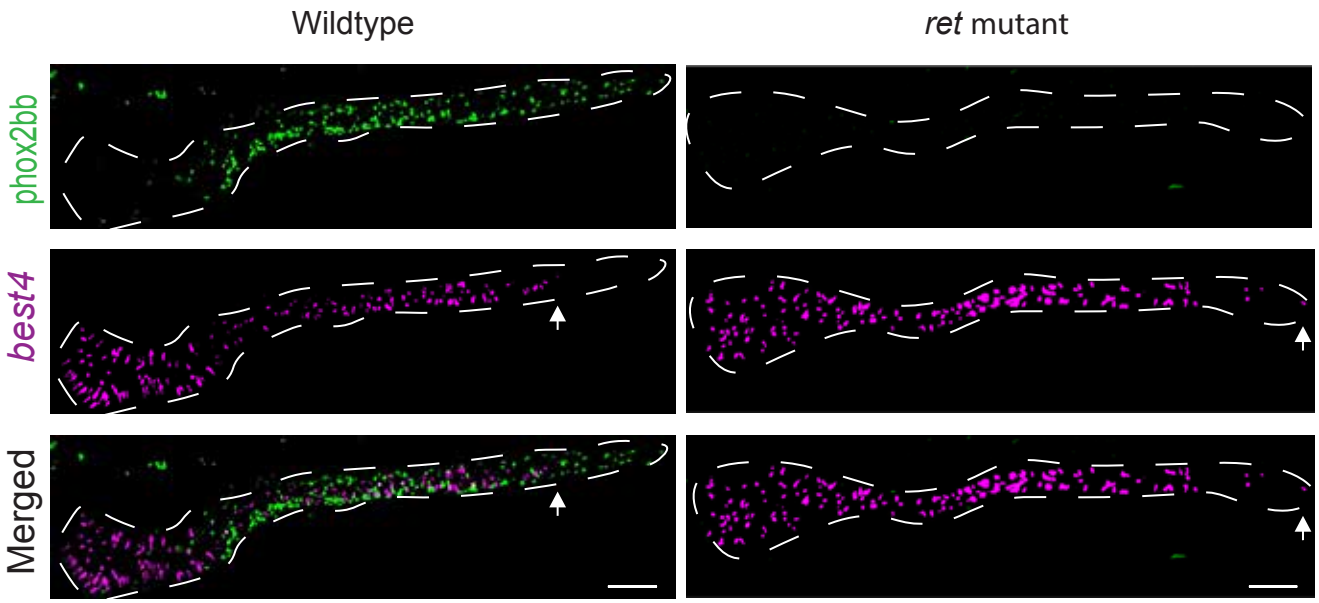
Wildtype
ret mutant
phox2bb
best4
Merged

C

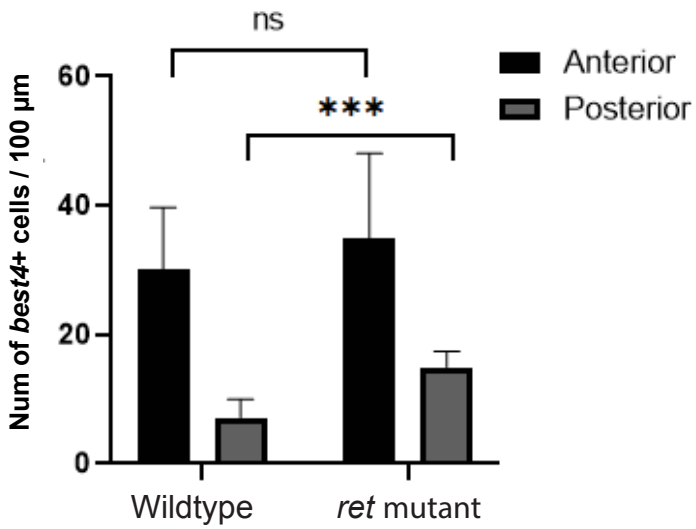
ns
***
Anterior
Posterior
Num of best4+ cells / 100 µm
60
40
20
0
Wildtype
ret mutant

Figure 6

A

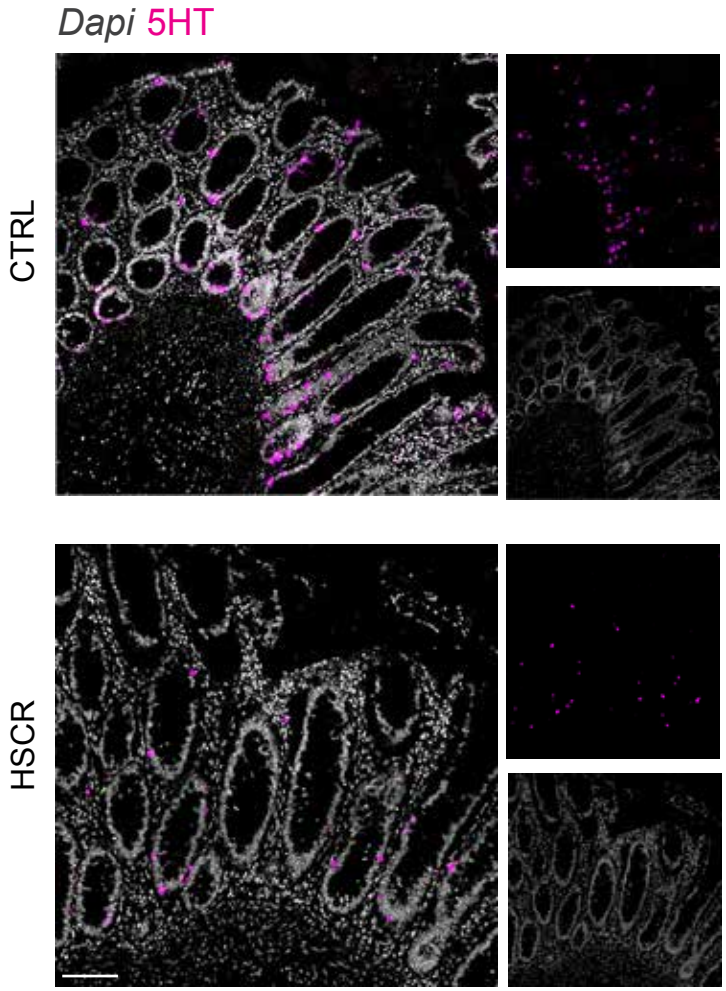

B

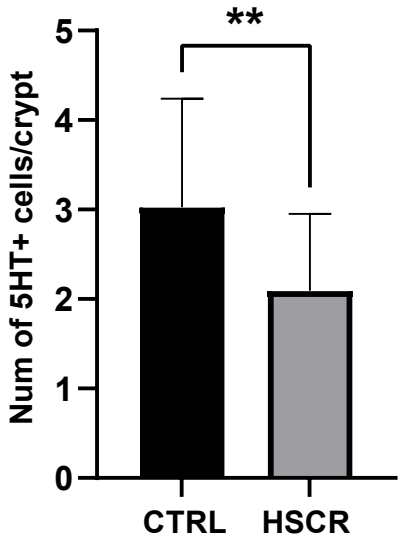

C

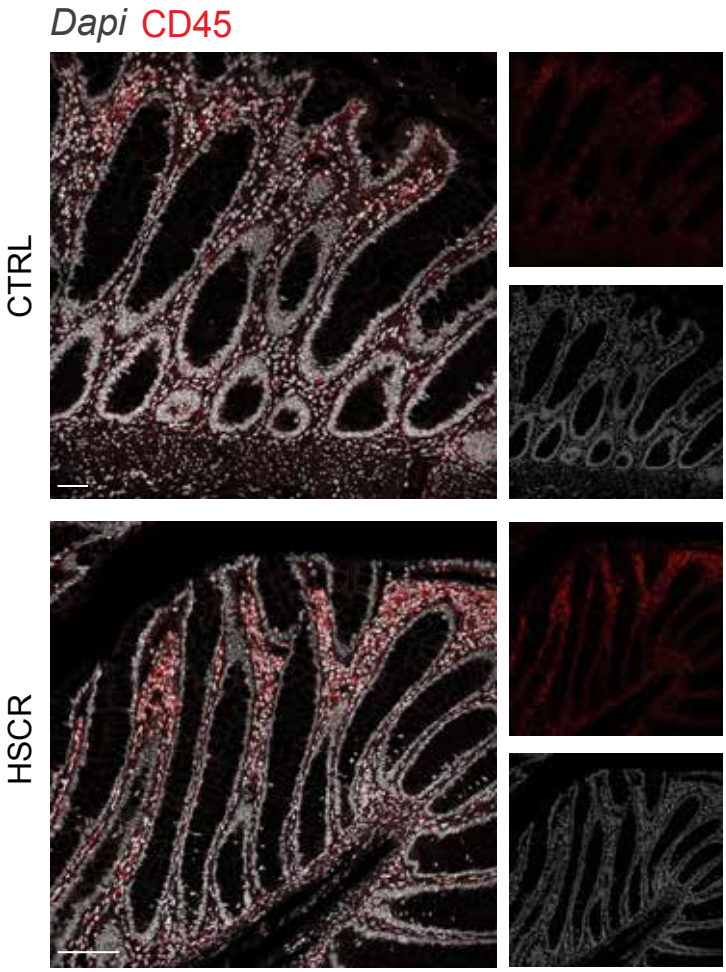

D

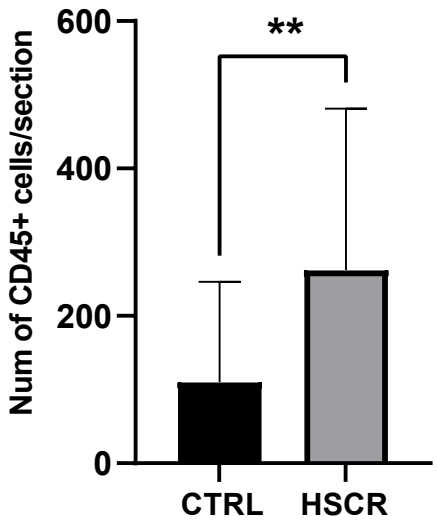

Figure 7

A

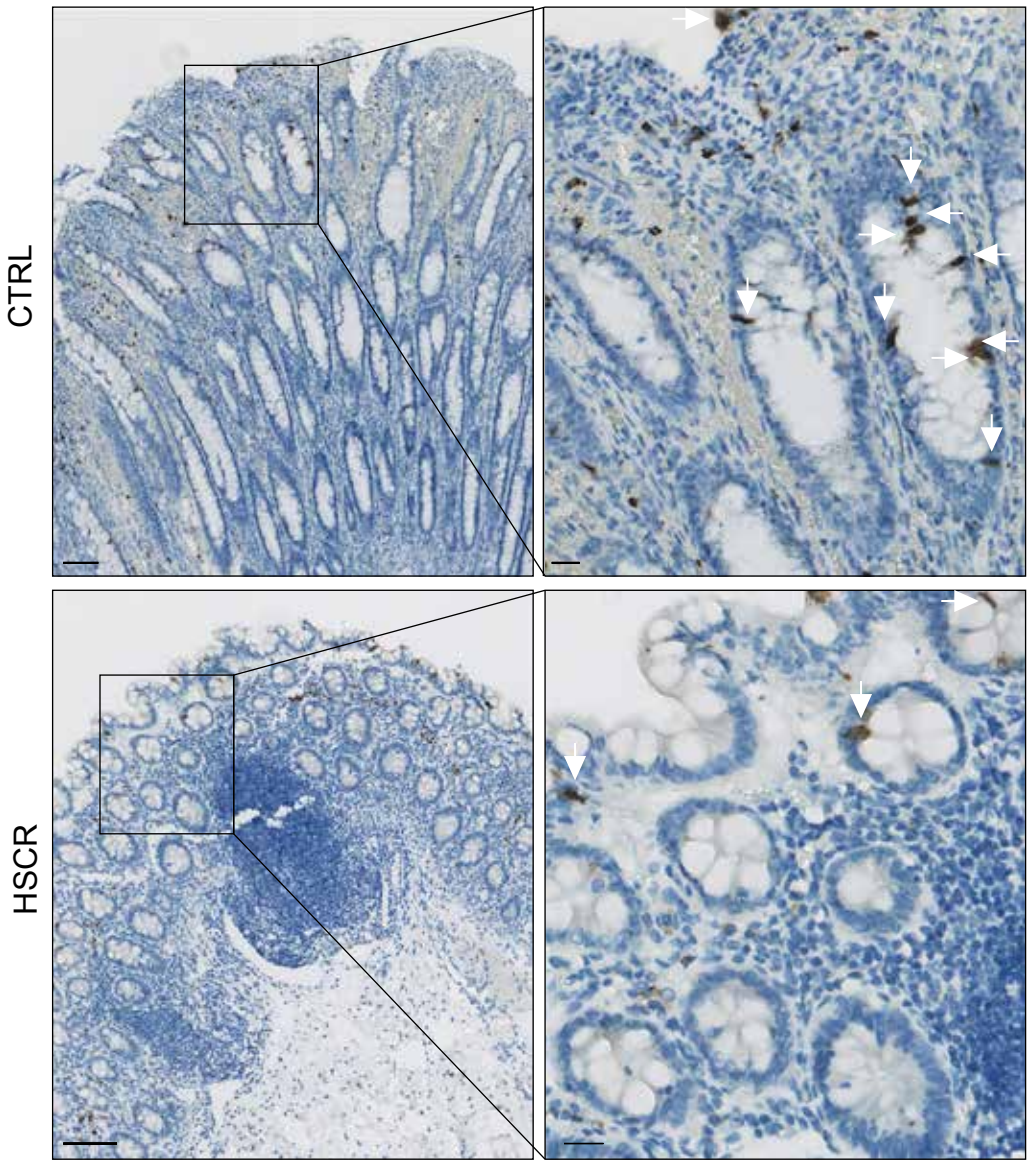
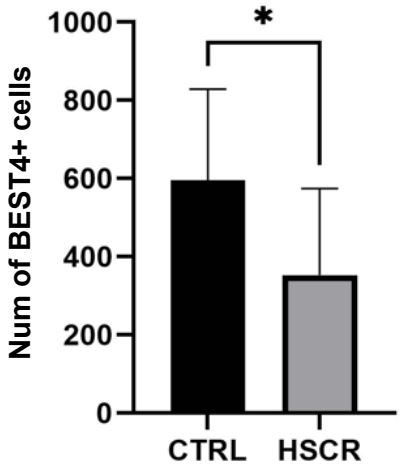
B